Local and Bi-Global Stability Analysis of a Plasma Actuated Boundary Layer

Mark Riherd* and Subrata Roy†

Applied Physics Research Group, University of Florida, Gainesville, FL, 32611

Local and bi-global stability methods have been employed to examine the effects of flow-wise oriented dielectric barrier discharge actuators on a laminar, zero pressure gradient boundary layer. Both methods indicate that the Tollmien-Schlichting wave is stabilized when plasma actuators are used to add momentum into the boundary layer. The general behavior of boundary layer stabilization is consistent with experimental results. In addition to examining the hydrodynamic stability properties explicitly, elementary flow characterization has also been performed. This flow characterization is performed in order to better understand the changes to flow stability implicitly through the changes to shape factor and boundary layer heights caused by the use of plasma actuation.

Nomenclature

u, v, w	Flow velocities
p	Pressure
$\bar{u}, \bar{v}, \bar{w}$	Mean flow velocities
$\bar{p}$	Mean pressure
$\tilde{u}, \tilde{v}, \tilde{w}$	Disturbance flow velocities
$\tilde{p}$	Disturbance pressure
u', v', w'	Complex disturbance flow velocities
p'	Complex disturbance pressure
u_∞	Freestream velocity
u_p	Induced velocity
α	Complex spatial frequency in x
β	Complex spatial frequency in z
ω	Complex temporal frequency
$\delta_{99\%}$	Boundary layer height
δ^*	Displacement boundary layer height
θ	Momentum boundary layer height
H	Shape factor ($H = \delta^*/\theta$)
Re	Reynolds number
γ	Velocity ratio
F	Dimensionless frequency, $F = \omega_R/Re$
Subscript	
i	direction
I	Imaginary
R	Real
S	Inflection point value

*Graduate Research Assistant, Student Member AIAA.

†Associate Professor, Associate Fellow AIAA

I. Introduction

The process of a flow's transition from laminar to turbulent has long been a topic of study in fluid mechanics. Specifically, the flow over a flat plate with zero pressure gradient (ZPG) is particularly important, as it shares many characteristics of other more complex flows. One instability present in this flow, characterized as the Tollmien-Schlichting (TS) wave, was first theoretically explored by Tollmien in 1929[1] and Schlichting in 1933,[2] and later experimentally verified by Schubauer and Skramstead in the 1940's.[3] While other instabilities and transition paths are known to exist and to also be of importance, the TS wave is the instability that is most closely tied to the controlled transition of turbulence.

This study examines the effect of using flow-wise operated dielectric barrier discharge (DBD) actuators on the stability of the ZPG boundary layer flow by modifying the TS wave. These devices are able to produce charged particles and a sufficiently strong electric field, which introduces a localized electrohydrodynamic body force that can be used to add or remove momentum from the nearby fluid.[4–6] Furthermore, these devices can be operated in a steady or duty-cycled manner, allowing them to be implemented as components of active and passive flow control systems. This type of actuator has a number of beneficial properties. It can be flush mounted on a surface. The response of the device is on electrical (not fluidic) time scales. These actuators can be operated over a very wide range of frequencies, ranging from Hertz (with duty cycling) or 100's of Hertz (without duty cycling) up to 10's of kiloHertz. The primary downside of this type of actuator is that it is only able to exert limited control authority, due to a weak plasma-flow coupling. The body force has only been able to generate velocities of up to 8 to 10 m/s under quiescent conditions.

In recent years, a number of studies have illustrated that this type of plasma device is useful for transition delay. Grundmann and Tropea[7,8] used these devices in a pulsed manner as a method of active transition delay as part of a closed loop control system to cancel oncoming TS waves. They found that DBD actuators could be used to accurately inject momentum into the boundary layer, modifying the TS waves. Furthermore, that group also used the actuators in a continuous manner in order to damp oncoming TS waves,[8] which they also had success with. Gibson[9] used DBD devices in a passive manner in conjunction with boundary layer suction to reduce the displacement and momentum deficit boundary layer heights and stabilize the flow. Duchmann et al[10] used these devices in a using continuous actuation and was able to capture the TS wave with and without plasma actuation using particle image velocimetry.

Aside from experimentation, some theoretical work has also been performed describing how the momentum addition using electrical devices modifies the boundary layer and its stability properties. Limited linear stability theory (LST) was performed and verified numerically and experimentally by Duchmann et al[11] when the actuator was placed within the transitional Reynolds number regime and operated continuously. This study further confirmed that there are distinct changes in the flow stability near the plasma device, but forgoes discussion a very in dept discussion of the effects.

Riherd and Roy[12] examined the various effects that could occur for an approximated boundary layer velocity profile, for both co-flow and counter flow operation of the plasma actuator. In their one-dimensional stability analysis, they discovered two previously undocumented boundary layer instabilities, though it did leave open certain questions with regard to potential bi-global stability modes and the accuracy of certain assumptions.

For the slowly developing, nearly parallel boundary layer, simple local stability analysis have been successful in predicting the linear stability properties of the flow. Methods using a parabolized form of the Navier-Stokes equations,[13] or direct numerical simulation[14] have produced similar results as the local stability analysis. This result suggests that a local stability analysis should work for the present boundary layer flow as well. However, in the region directly around the flow control actuator, the assumptions of a slowly developing, parallel flow are not be strictly satisfied, and there may be significant variations between properties of the local and global stability modes. In order to discern any potential two dimensional effects in the region of the flow control actuator, both local and bi-global stability analyses have been performed on the flow.

The goal of this study is to better understand the effects of implementing plasma actuation in a laminar boundary layer. For the local stability analysis, boundary layer profiles and flow fields are taken directly from simulated flows. Furthermore, the effects of a fully two dimensional flow field are examined, allowing for a better understanding of any localized effects. The results indicate that as the magnitude of the plasma actuation is increased, the boundary layer is stabilized. Based on the modifications to the base flow, two mechanisms are suspected to be causing this stabilization. The first of which is the addition of momentum into the boundary layer, reducing the boundary layer heights. The second is modifications to the boundary

layer velocity profile, which implicitly change the shape factor and the onset of instabilities.

In order to quantify the modifications of the boundary layer's stability, both local and bi-global stability methods have been employed. For moderate levels of plasma actuation, local stability analysis predicts that the critical Reynolds number of the Tollmien-Schlichting wave is increased from $Re_{x,crit} \approx 92,500$ ($Re_{\delta^*,crit} \approx 520$) to $Re_{x,crit.} > 160,000$ ($Re_{\delta^*,crit.} > 700$). Stabilization of the TS wave is also predicted when bi-global stability methods are employed. Using bi-global stability methods, changes to the shape and reduction in the peak velocity magnitude of the TS wave are predicted.

II. Baseline Flow Modification

As a starting point for the stability analysis, the effect of the DBD actuation on the ZPG boundary layer have been simulated numerically. This is done using the Implicit Large Eddy Simulation (LES) Navier-Stokes solver FDL3DI.[15] A fine two dimensional mesh (801×151) is used, which resolved the near wall boundary layer, the effects of a sharp leading edge, and the steady addition of momentum through a body force term. At the location of plasma actuation, there are 62 points in the boundary layer ($\delta_{99\%}$) for the Reynolds number tested as part of this study. This mesh is finer than required and is able to capture the flow adequately near regions of high gradients, particularly for the thin boundary layer near the plate leading edge. The mesh is geometrically stretched near the boundaries in order to prevent the effects of reflections that could potentially bounce off of the far field boundaries and interfere with the flow. A schematic of the domain used can be seen in Fig. 1.

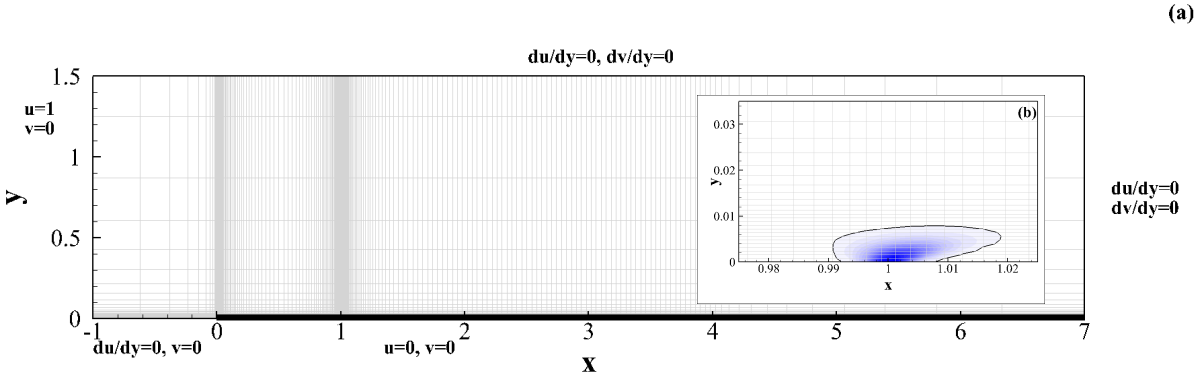

Figure 1. (a) The two dimensional domain used for the baseline flow modifications and (b) a close up of the x-component of body force injected into the boundary layer. Every fourth grid point is shown.

The plasma actuation is modeled using an approximate body force distribution based on first principle simulations of the plasma discharge[16] (Fig. 1 b) in a manner consistent with the description in Rizzetta et al.[15] While this model does lack some of the physical behavior that is better captured by first principle models,[17] it is not subject to the more rigorous computational demands or the very high frequency unsteady behavior that is normally damped out by the boundary layer. The magnitude of the body force required to produce a wall jet under quiescent conditions of a specified velocity was determined a priori. The same set up was used with no slip conditions ($u = v = 0$) for the left, right, and bottom boundaries and a no shear condition on the upper boundary, leading to a quiescent condition over a majority of the domain. The plasma actuator is run at various magnitudes with quiescent initial and a mix of no slip/no shear boundary conditions. The effect of the actuation on the flow is then characterized by the maximum velocity seen in the wall jet (u_p, shown in Fig. 2). A linear interpolation was then used to control the body force for the simulation under non-quiescent conditions. The magnitude of the implemented force is characterized by the non-dimensional parameter

$$\gamma = \frac{u_p}{u_\infty} \tag{1}$$

This parameter is selected in order to focus solely on the fluid dynamic effect of the plasma actuation and its influence on the flow stability, ignoring the electrical inputs such as voltage, frequency and the waveform driving the device. The values of γ are calibrated for the Reynolds number tested as part of this study.

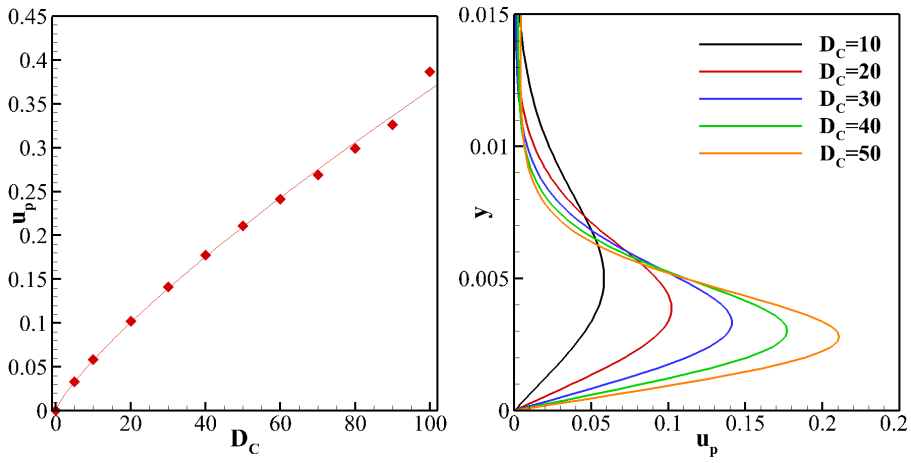

Figure 2. (a) Values of u_p used to calibrate D_c. (b) Velocity profiles at a location downstream of the plasma actuation for various values of D_c.

In the simulations, the body force was placed at a position corresponding to $Re_x = 100,000$ ($Re_{\delta^*} = 543$) in a boundary layer flow. This actuator location is the transitional regime, which is useful for understanding how the momentum addition modifies the laminar to turbulent transition in the critical domain.

The first thing that should be noticed is that the addition of momentum into the boundary layer modifies the boundary layer profiles. Slightly upstream of the actuator, the flow is pulled downwards into the wall as if there were boundary layer suction present (Fig. 3 a and d). Immediately downstream of the device, the boundary layer profile shows several inflection points, which suggests that inviscid instabilities may become important (Fig. 3 b and e), as they satisfy Fjørtoft's criteria.[18] Further downstream of this, the profiles return to something resembling the Blasius profile, though thinner than that of the initial flow (Fig. 3 c and f).

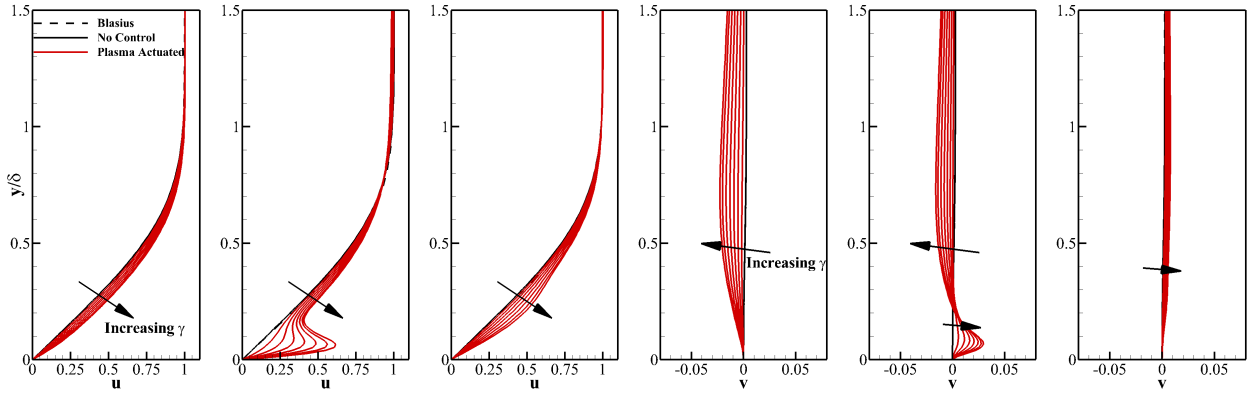

(a) $u, x = 0.99$ (b) $u, x = 1.01$ (c) $u, x = 1.10$ (d) $v, x = 0.99$ (e) $v, x = 1.01$ (f) $v, x = 1.10$

Figure 3. Boundary layer velocity profiles as a function of the velocity ratio, γ at locations upstream (a,d), directly downstream (b,e) and downstream (c,f) of the actuator. The rapid development of suction and wall jet effects and the gradual diffusion of momentum in the boundary layer can be seen to increase in magnitude as the value of γ is increased.

As the boundary layer velocity profiles are modified due to actuation, the displacement and momentum deficit of the boundary layer should be altered as well. It can be seen in Fig. 4 that there is a monotonic response of the boundary layer heights to the magnitude of the body force. There are some localized effects near the boundary layer, in which the boundary layer height may rise ($\delta_{99\%}, \theta$) due to modifications very near to or away from the wall or fall (δ^*) due to a reduction in the boundary layer momentum deficit. Overall,

there is a drop in the boundary layer heights downstream with the addition of momentum into the boundary layer.

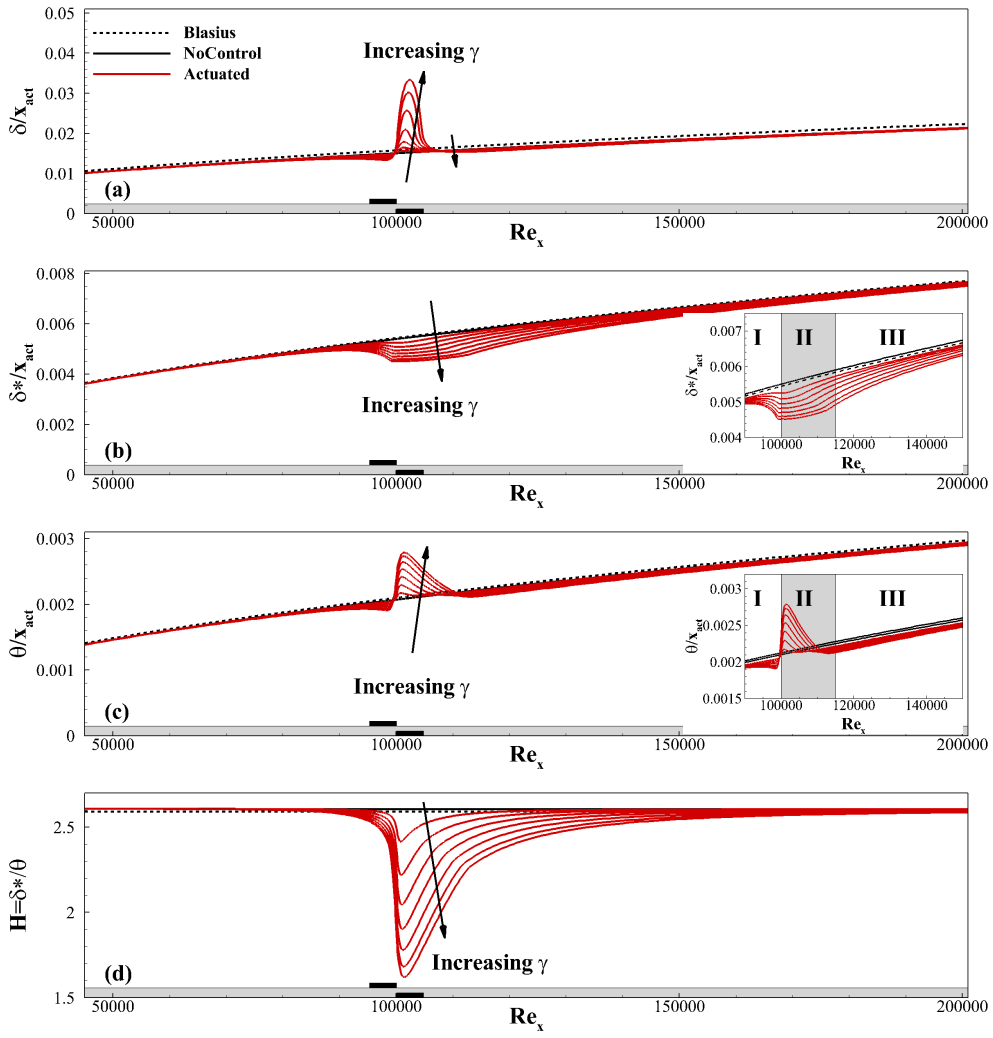

Figure 4. Boundary layer heights as a function of the velocity ratio, γ, for values ranging from 0 to 0.35, with a spacing of 0.05 - (a) $\delta_{99\%}$, (b) δ^*, (c) θ, and (d) the shape factor, $H = \delta^*/\theta$, along with a comparison to the analytical solution for the case of $Re_{act} = 100,000$. Inlays show a zoomed in view near the actuator location.

All of these effects suggest that there are 3 different locations important to the stability of these devices. There is the region upstream of the devices (I), which may now be slightly more stable due to boundary layer suction. There is the region over and immediately downstream of the device (II), which shows signs of inviscid instability due to Fjørtofts criteria. Finally, there is the region far downstream of the device (III), which should be more stable due to a reduced boundary layer height caused by the injection of momentum into the boundary layer by the plasma actuator. These simulations of the plasma actuation in the co-flow orientation show that there are a number of different spatial regions within the flow field.

III. Local Linear Stability Theory

A. Numerical model of the eigenvalue problem

Linear stability theory can be used to predict the existence and growth rates of instabilities that may manifest themselves in the boundary layer. For this local stability analysis, temporal instabilities are examined, though with the Gaster transformation, the spatial instabilities could also be examined.[19]

In order to perform this type of analysis, it must be assumed that the flow is slowly developing and

parallel to the surface. Two metrics have been developed by Riherd, Roy and Balachandar,[20] $E_{\parallel}$ and E_d, which quantify the validity of these assumptions. These metrics are defined as

$$E_{\parallel} = \tan^{-1}\left(\max_{y\in(0,\infty)}\left|\frac{\bar{v}}{\bar{u}}\right|\right) \tag{2}$$

and

$$E_d = \max_{y\in(0,\infty)}\left|\frac{\partial \bar{u}}{\partial x}\right| \tag{3}$$

and quantify the parallel flow and slowly developing assumptions, respectively. These assumptions are quantified in Fig. 5. This flow, while it does exhibit some rapid spatial changes and non-parallel behavior near the actuator, can be considered a slowly developing, parallel flow over the remainder of the domain. As such, one dimensional linear stability theory can be applied, except for near the actuator. In order to understand the effects near the actuator, a bi-global stability method is employed, the results of which are discussed in section IV.

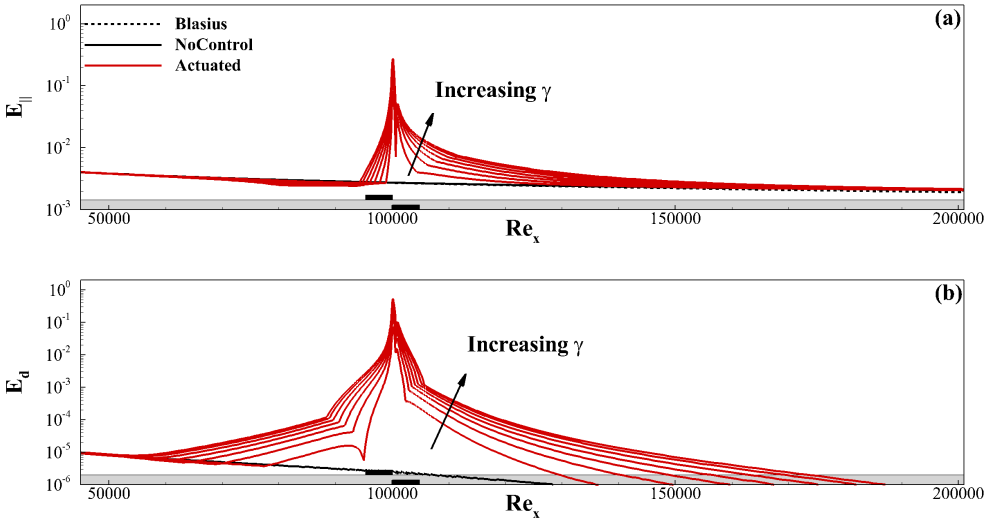

Figure 5. Evaluation of (a) $E_{\parallel}$ and (b) E_d for the flow fields calculated in section II for velocity ratios of $\gamma = 0$ to $\gamma = 0.35$.

The formulation of the present local stability analysis begins with the linearized Navier-Stokes equations,

$$u_i = \bar{u}_i + \tilde{u}_i, p = \bar{p} + \tilde{p} \tag{4}$$

$$\frac{\partial \tilde{u}_i}{\partial x_i} = 0 \tag{5a}$$

$$\frac{\partial \tilde{u}_i}{\partial t} + \bar{u}_j\frac{\tilde{u}_i}{\partial x_j} + \tilde{u}_j\frac{\bar{u}_i}{\partial x_j} + \frac{\partial \tilde{p}}{\partial x_i} - \frac{1}{Re_{\delta_0^*}}\frac{\partial^2 \tilde{u}_i}{\partial x_j^2} \approx 0 \tag{5b}$$

It should be noted that the non-dimensionalization here is now based on δ_0^*, which is the boundary layer height of the non-actuated case at a given location in x rather than x_{act} as it was done in the previous section.

The problem can be further simplified if several assumptions are made. First, assume that all of the disturbance quantities are wavelike in nature and can be split into the produce of a disturbance profile normal to the surface (y) and a wave travelling in the streamwise (x) and spanwise (z) directions such that

$$\tilde{\phi} = \phi'(y)\exp\left(i\left(\alpha x + \beta z - \omega t\right)\right) \tag{6}$$

where α, β, and ω are the angular wave numbers in x, z, and time. From this point onward, let $i = \sqrt{-1}$. Also assume that a slow developing flow can be approximated as a 1D mean flow ($\overline{v} = \overline{w} = \frac{\partial\overline{(\cdot)}}{\partial x} = \frac{\partial\overline{(\cdot)}}{\partial z} = 0$). With these assumptions, the problem can be formulated as the following generalized eigenvalue problem:

$$i\alpha u' + \frac{\partial v'}{\partial y} + i\beta w' = 0 \tag{7a}$$

$$i\alpha\bar{u}u' + v'\frac{\partial\bar{u}}{\partial y} + i\alpha p' - \frac{1}{Re}\left(-\alpha^2 u' + \frac{\partial^2 u'}{\partial y^2} - \beta^2 u'\right) = i\omega u' \tag{7b}$$

$$i\alpha\bar{u}v' + \frac{\partial p'}{\partial y} - \frac{1}{Re}\left(-\alpha^2 v' + \frac{\partial^2 v'}{\partial y^2} - \beta^2 v'\right) = i\omega v' \tag{7c}$$

$$i\alpha\bar{u}w' + i\beta p' - \frac{1}{Re}\left(-\alpha^2 w' + \frac{\partial^2 w'}{\partial y^2} - \beta^2 w'\right) = i\omega w' \tag{7d}$$

This set of equations (Eqns. 7a - 7d) was then discretized onto a uniform staggered mesh. The velocity data was stored at and the momentum equations evaluated at the points coincident with the boundary layer. The pressure data was stored at and the continuity equation evaluated at the intermediate points. A 4^{th} order accurate, centered finite difference stencil was used for the differencing over a majority of the domain. A 2^{nd} order accurate, centered finite difference scheme was used at the boundaries. Boundary layer profiles from the simulations in Section **II** were interpolated onto the uniform mesh. The eigenvalues and eigenvectors were then calculated using MATLAB's `eig` function.[21]

B. Co-Flow Actuation

Velocity profiles from Section **II** were extracted from 160 points in the flow ($0 < Re_x < 4Re_{act}$) and examined using the eigenvalue analysis as provided. Only the non-oblique modes have been examined ($\beta = 0$). Sufficiently far upstream of the flow modification, the stability properties are unchanged. However, the stability is modified in the regions near and downstream of the body force. The extracted eigenvalues for the case of $Re_{act} = 100,000$ at $Re_x = 120,000$ can be seen in Fig. 6. The critical eigenvalue moves monotonically from unstable to stable as γ increases (Fig. 6b). Stability diagrams are shown in Fig. 7 for the different values of γ examined. Again, a monotonic behavior is found to exist, where the higher levels of actuation have a more profound effect on the stability characteristics (either stabilizing or destabilizing depending on the specific eigenmode). It can be seen that as the value of γ and amount of momentum transfer is increased, the 'thumb' region typically associated with instabilities in the ZPG boundary layer is moved farther and farther downstream. This indicates that the boundary layer stability is successfully being reinforced by the use of DBD actuation.

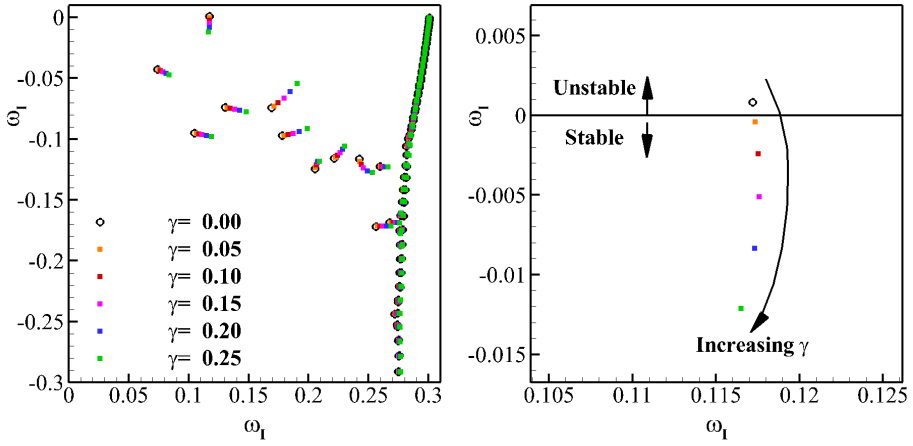

(a) Computed eigenspecta (b) Close-up of the critical eigenvalue

Figure 6. Computed eigenvalues for the case of $Re_{act} = 100,000$ at $Re_x = 120,000$, $\alpha = 0.3$ (a). A close-up of the TS wave eigenvalue is also shown (b).

It can be seen that LST predicts increased flow stabilization in terms of Re_x (Fig. 8) as well as $Re_{\delta*}$ in the neutral stability curves (Fig. 7). Furthermore, this flow stabilization extends beyond the near actuator region, to points where the assumptions required for the one-dimensional stability analysis are valid. The reasons for this flow stabilization are likely to be due to two different effects, both of which are coupled to each other and the addition of momentum into the boundary layer. The addition of momentum into the boundary layer is shown to reduce the boundary layer displacement height (as shown in Fig. 4 b). In turn,

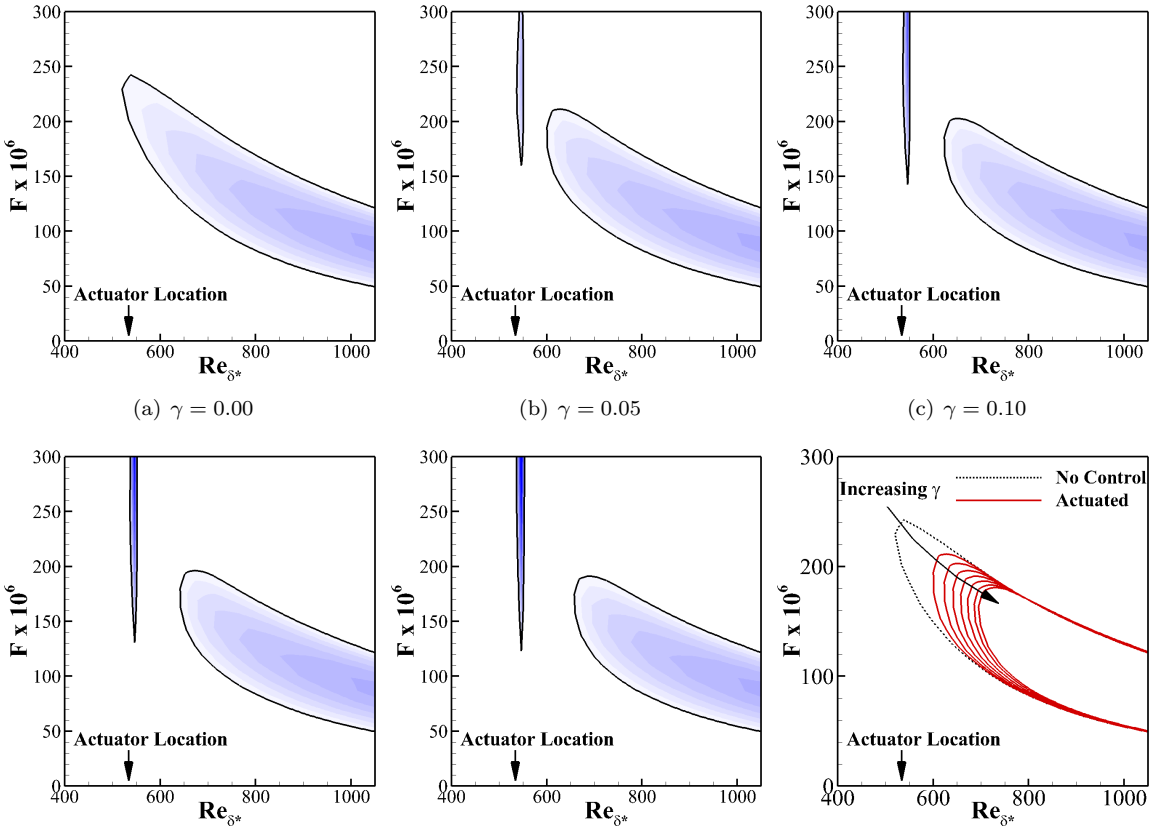

(a) $\gamma = 0.00$ (b) $\gamma = 0.05$ (c) $\gamma = 0.10$

(d) $\gamma = 0.15$ (e) $\gamma = 0.20$ (f) Neutral stability curve

Figure 7. Stability diagrams of the flows when the actuator is placed at $Re_x = 100,000$. In (a)-(e), the line of neutral stability is marked. $F = Real(\omega)/Re_{\delta^*}$. (f) Neutral stability curves for values of γ ranging from 0.00 to 0.35 with a spacing of 0.05

this reduces the local boundary layer Reynolds number, which delays the onset of perturbation growth in the boundary layer. The second source of stabilization results from the momentum addition modifying the boundary layer velocity profiles (as shown in Fig. 3). By modifying the boundary layer profiles, the shape factor ($H = \delta^*/\theta$) is modified. This parameter has been shown to be very important in identifying the onset of the perturbation growth in boundary layers through a "universal correlation,[22]" where a decreased shape factor implies transition delay of the TS wave. Fortunately, the manner in which momentum is added into the boundary layer reduces the shape factor, thus delaying the critical onset of the TS wave's growth.

IV. Bi-Global Stability Theory

The set of assumptions required for these one-dimensional calculations are not strictly satisfied by the flow fields generated, particularly the assumptions of a fully developed and a parallel flow field (Fig.5). In order avoid the restrictions imposed by these assumptions, the fully two-dimensional flow field can be considered instead, though not without significant computational expense.

Bi-global stability starts with the same linearized Navier-Stokes equations as the local stability theory, but the perturbation takes the more general form of

$$\tilde{\phi} = \phi'(x, y) \exp\left(i\left(\beta z - \omega t\right)\right) \tag{8}$$

Substituting this form of the perturbation into the linearized incompressible Navier-Stokes equations, the following system of equations is arrived at

$$\frac{\partial u'}{\partial x} + \frac{\partial v'}{\partial y} + i\beta w' = 0 \tag{9a}$$

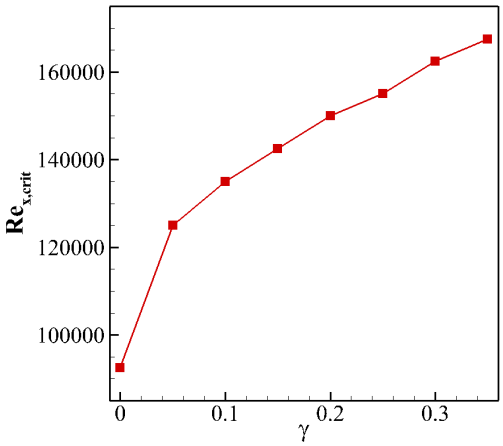

Figure 8. Critical values of Re_x for the actuated flow.

$$\bar{u}\frac{\partial u'}{\partial x} + \bar{v}\frac{\partial u'}{\partial y} + \bar{w}i\beta u' + u'\frac{\partial \bar{u}}{\partial x} + v'\frac{\partial \bar{u}}{\partial y} + \frac{\partial p'}{\partial x} - \frac{1}{Re}\left(\frac{\partial^2 u'}{\partial x^2} + \frac{\partial^2 u'}{\partial y^2} - \beta^2 u'\right) = i\omega u' \tag{9b}$$

$$\bar{u}\frac{\partial v'}{\partial x} + \bar{v}\frac{\partial v'}{\partial y} + \bar{w}i\beta v' + u'\frac{\partial \bar{v}}{\partial x} + v'\frac{\partial \bar{v}}{\partial y} + \frac{\partial p'}{\partial y} - \frac{1}{Re}\left(\frac{\partial^2 v'}{\partial x^2} + \frac{\partial^2 v'}{\partial y^2} - \beta^2 v'\right) = i\omega v' \tag{9c}$$

$$\bar{u}\frac{\partial w'}{\partial x} + \bar{v}\frac{\partial w'}{\partial y} + \bar{w}i\beta w' + u'\frac{\partial \bar{w'}}{\partial x} + v'\frac{\partial \bar{w'}}{\partial y} + i\beta p' - \frac{1}{Re}\left(\frac{\partial^2 w'}{\partial x^2} + \frac{\partial^2 w'}{\partial y^2} - \beta^2 w'\right) = i\omega w' \tag{9d}$$

If the system is driven by an external forcing, such as free stream turbulence or oscillations on the surface of the plate, then it can be reduced to

$$\frac{\partial \mathbf{u}}{\partial t} = \mathbf{A}\mathbf{u} + \mathbf{f} \tag{10}$$

where $\mathbf{f}$ contains the information regarding the external perturbations. Assuming a periodic solution, this can be reduced to

$$(i\omega\mathbf{B} - \mathbf{A})\,\mathbf{u} = \mathbf{f} \tag{11}$$

In this form, the effect of specific perturbations on the flow can be examined.

A. Numerical method and boundary conditions

The system of equation for the bi-global stability analysis was solved on a half-staggered mesh. The momentum equations are solved and velocity data stored on a mesh of points that is coincident with the boundaries of the domain. The continuity equation and pressure data are stored on intermediate points. This configuration allows for boundary conditions for pressure to be neglected, as the pressure is only necessary to ensure that the continuity equation is enforced for incompressible flows, and is not solved at the boundaries at present.

For many bi-global stability applications (especially those involving eigen-spectra or optimal perturbations), the size of the differentiation matrix can determine whether or not the method is computationally feasible, even with large scale computational resources. In order to minimize the size of the differentiation matrix (i.e. $\mathbf{A}$ and $\mathbf{B}$), higher order, higher resolution methods have been implemented. In the x-direction, 4th order accurate, centered stencils were used, except for the $\bar{u}\frac{\partial(\cdot)}{\partial x}$ term, which used a 3rd order accurate, upwind biased stencil. Due to the outlet boundary condition, some reflections are able to propagate back upstream (using interpolation or a Gaster type outlet condition). This leads to error waves being generated in the flow field. These waves are damped out with the use of the upwind stencil, which includes a small amount of artificial dissipation at higher spatial frequencies. In the y-direction, a Chebyshev collocation method is employed for the differentiation and interpolation.

For the outlet boundary conditions and the free stream boundary conditions, a low order interpolation is employed. This interpolation allows for the perturbation to flow more freely out of the domain without

sending spurious waves upstream. The form of this low order interpolation is

$$\phi_N = u_{N-1} + \left.\frac{\partial \phi}{\partial x}\right|_{x_{N-1}} (x_N - x_{N-1}) \tag{12}$$

In addition to this, a region of low order upwinding is used in the final 1/8 of the domain. This upwinded region forms a buffer region at the exit of the domain, which further prevents reflections from propagating upstream from the outlet.

For the boundary conditions, a TS wave is enforced at the inlet. As the frequency (ω_R) is varied, so is the shape of the wave. This boundary condition is generated using the one-dimensional stability analysis described in section III for each frequency tested. The resulting eigenmode from the local stability analysis is then interpolated onto the collocation mesh. This boundary condition is the one that drives the flow and is implemented through the forcing term **f** in Eqn. 11.

B. Influence of domain length

Calculations of the system response with no actuation indicate that the incoming TS wave propagates downstream, growing and decaying in the magnitude of the perturbation, as well as becoming taller as the boundary layer thickens. However, it does appear that the length of the domain matters in determining the growth of the perturbations. Three different domain lengths have been examined, the lengths and grid spacings of which are shown in Table 1. The grid spacing is not constant, though the variations in Δx are less than 20%. It can be seen in Fig. 9 that there are variations in the response depending on the domain length. However, for the longest length, which stretches approximately 531 inlet displacement boundary layer heights, the results should be independent enough of the length to make reasonable comparisons with other results.

Case	$Re_{\delta^*,in}$	$Re_{\delta^*,out}$	L_x	n_x	Δx	Δy_w
Small	300	450	126.6	257	0.495	0.0308
Medium	300	600	303.9	513	0.594	0.0308
Large	300	750	531.9	1025	0.519	0.0308

Table 1. Comparison of domain and grid parameters for three test cases involving the Blasius boundary layer.

C. Blasius Boundary Layer

In order to evaluate the accuracy of the method, the results from the Large domain have been examined. The results indicate that in spite of the efforts to minimize reflections and oscillations, some do still exist, and their presence can be seen in the unsmoothed neutral stability curve and growth rates (Fig. 10a). The results of these calculations do not match perfectly with traditional 1D, but are more comparable to those of developing boundary layer flows, such as the results of Gaster.[23]

D. Plasma Modified Boundary Layers

Knowing that the present bi-global stability code provides approximately correct results, plasma modified boundary layers can now be examined. The region of plasma actuation is shown in Fig. 11. These flow fields and their velocity gradients are then interpolated onto a coarser mesh for the stability calculations. The resolution of this flow field may be a weak point in the calculations. The sharper gradients in the base flow may not be reflected in the response due to insufficient resolution. However, with 1025 points in the x-direction, and 41 collocation point (using spectral differencing) in the y-direction, the program uses upwards of 6 GB of memory for the calculations. To work with a higher resolution than this is simply not possible at the current time.

The response of the system (Fig. 12) shows that the incoming TS wave is changed by the plasma actuation. There are localized effects near the plasma actuator, but the incoming TS wave does not show any dramatic changes as it passes over the actuator. The shape of the wave is skewed, but it can still be reasonably referred to as a TS wave, and not some new instability mode. It can be seen in Fig. 12 that as

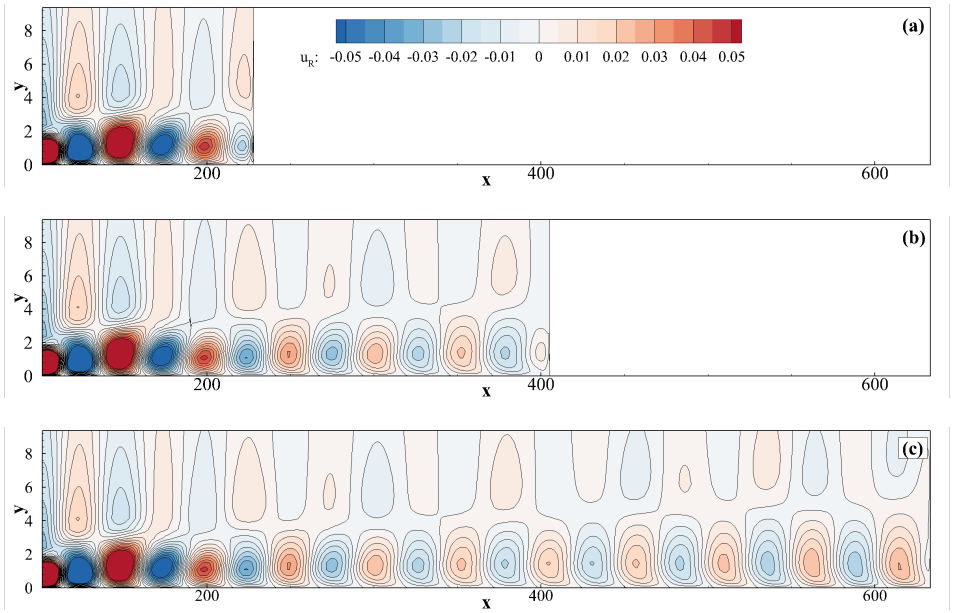

Figure 9. Comparison of the real portion of the u-velocity for the (a) short, (b) medium, and (c) long domains examined for the frequency of $\omega_r = 0.0445$ $\left(F \times 10^6 = 148.3\right)$

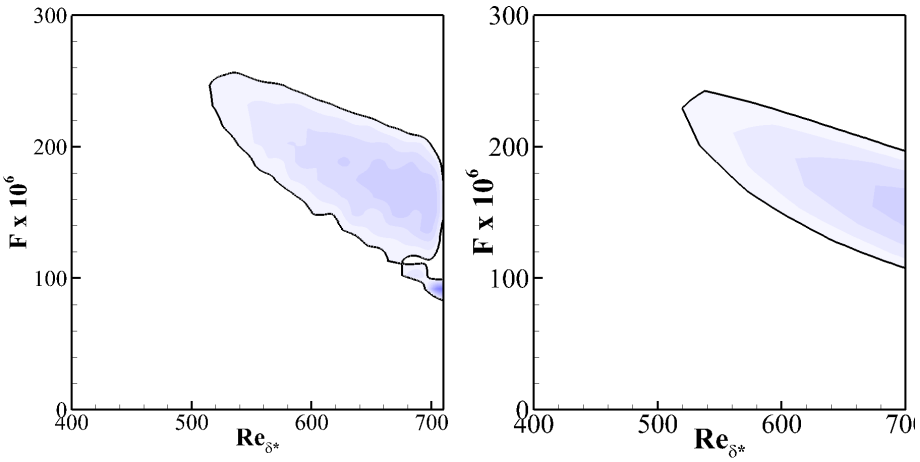

(a) Bi-global (b) Local

Figure 10. The neutral stability regions as calculated by the (a) bi-global stability method, and using the growth of the maximum streamwise velocity in the streamwise direction and (b) for the local stability method, using the imaginary part of the eigenvalue. The unstable region is colored by the growth rates (i.e. negative values of α_i for the bi-global method and positive values of ω_i for the local method).

the magnitude of the plasma actuation (i.e. the value of the velocity ratio) is increased, the T. S. wave is lengthened. This lengthening of the TS wave indicates that the phase speed of the wave is increased, which is consistent with previous experimental results[10] and with the momentum addition increasing the average velocity in the boundary layer. Of greater importance, is the observation that the maximum value of the streamwise velcocity component is reduced. This indicates that the plasma actuation is locally stabilizing the boundary layer (Fig. 13). Based on the maximum streamwise velocity component, at certain frequencies, the TS wave can be reduced in magnitude by up to 50%.

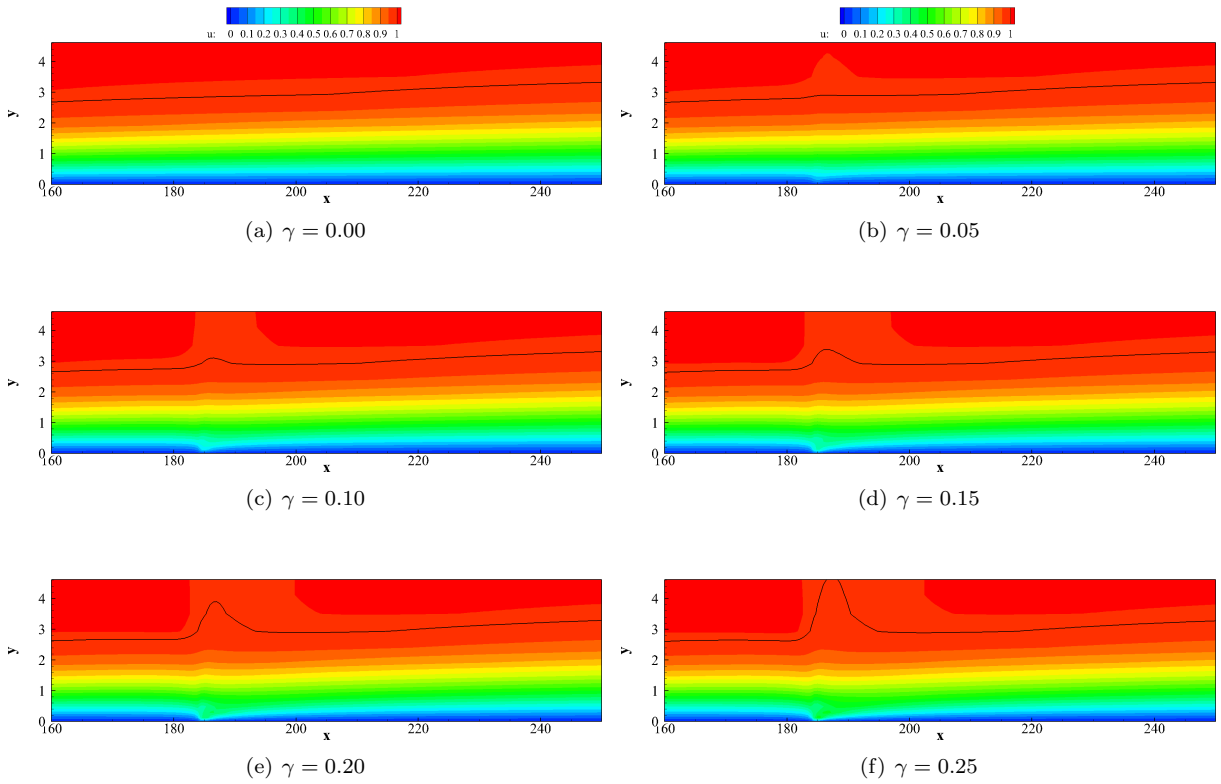

(a) $\gamma = 0.00$ (b) $\gamma = 0.05$

(c) $\gamma = 0.10$ (d) $\gamma = 0.15$

(e) $\gamma = 0.20$ (f) $\gamma = 0.25$

Figure 11. Flow fields near the plasma actuator for varying values of γ. The black line indicates where $u = 0.99u_\infty$.

V. Conclusions

The effects of using co-flow oriented DBD plasma actuators in a zero pressure gradient boundary layer on the laminar to turbulent transition process have been examined using local and bi-global stability tools. Focus of these stability analyses centers around the TS wave, which is the transition path most closely associated with the controlled boundary layer transition, though other transition paths are known to exist and to be of importance in many aerospace applications.

Simulations have been performed which model the introduction of momentum into the boundary layer using plasma actuation. Because of this momentum addition, the boundary layer may be stabilized for two different reasons. The momentum addition reduces the boundary layer heights, which in turn reduces the relevant Reynolds number of the boundary layer (Re_{δ^*}). In addition to changing the boundary layer heights, the shape factor of the boundary layer is also reduced (though only locally). Reduction of the shape factor implies an increase in the critical Reynolds number, further delaying the onset of perturbation growth in the boundary layer.[22]

Both of the stability tools used as part of this study predict that co-flow DBD actuation stabilized the boundary layer with respect to the TS wave. Neutral stability curves have been calculated using local stability analysis. Using the bi-global stability analysis, localized modifications to the TS wave have been found to exist and become more pronounced as the magnitude of the plasma actuation is increased.

While computational difficulties have been encountered in the use of bi-global stability analysis, the present results indicate that there are relatively rapid changes (over less than a single wavelength) in the shape of the TS wave. This result could not be achieved using a local stability analysis. While these computational difficulties must be overcome before high quality data for comparisons to experiments can be achieved, the present results seem promising and should lead to those results.

Future work in understanding the boundary layer transition control using this manner of plasma based control should focus on identifying the additional instability modes that have been hypothesized[12,20] along with progresses in the understanding, measuring, and controlling the present and more complex paths to

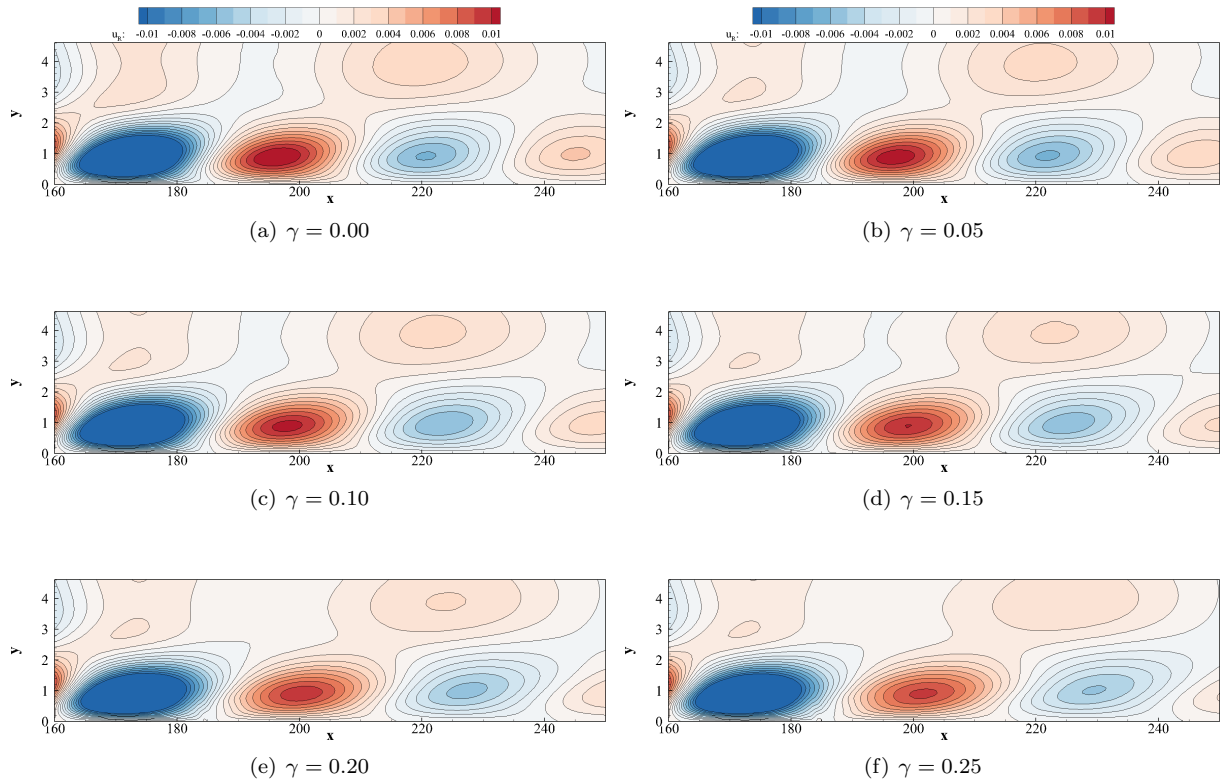

(a) $\gamma = 0.00$ (b) $\gamma = 0.05$

(c) $\gamma = 0.10$ (d) $\gamma = 0.15$

(e) $\gamma = 0.20$ (f) $\gamma = 0.25$

Figure 12. Response of the flow field to an incoming TS wave at the frequency $\omega_r = 0.0445$ $\left(F \times 10^6 = 148.3\right)$ for various values of γ. Note that the x and y scales are not the same.

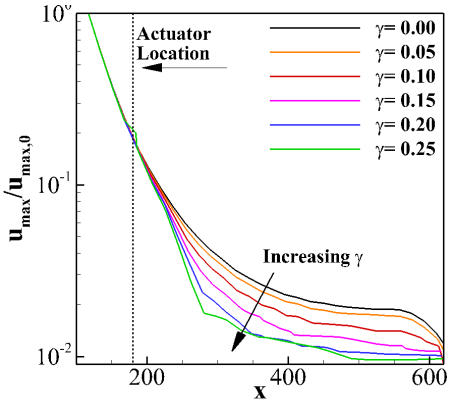

Figure 13. Relative amplitudes of the maximum value of u for a frequency of $\omega_R = 0.0694$ $\left(F \times 10^6 = 231.3\right)$. Values are normalized by the maximum value of u at the inlet for various values of γ.

transition. Additional numerical and/or experimental work should be performed in order validate the present calculations or the similar flow conditions examined experimentally by Tropea and his co-workers.[7,8,10,11] Work of this manner may helpful in identifying exactly what sub-domain of the flow require bi-global stability analysis and which domains local stability analysis is sufficiently accurate. In addition to the presently examined two dimensional TS wave, evaluating the control authority of plasma actuation with respect to the most amplified perturbations[24] would be of significant importance. This second path to turbulence is more closely related to transition under low disturbance conditions and control of it would be beneficial for many aerospace applications.

References

[1]Tollmien, W., "Über die Entstehund der Turbulenz," *Nachr. Ges. Wiss. Göttingen, Math.-Phys. Kl.*, 1929, pp. 21–44.

[2]Schlichting, H., "Zur Entstehung der Turbulenz bei der Plattenströmung," *Z. Angew. Math. Mech.*, Vol. 13, 1933, pp. 171–174.

[3]Schubauer, G. B. and Skramstad, H. K., "Laminar boundary-layer oscillations and transition on a flat plate," *Z. Angew. Math. Mech.*, Vol. 38, 1947, pp. 251–292.

[4]Roth, J. R., Sherman, D. M., and Wilkinson, S. P., "Electrohydrodynamic Flow Control with a Glow-Discharge Surface Plasma," *AIAA Journal*, Vol. 38, 2000, pp. 1166–1172.

[5]Corke, T. C., Enloe, C. L., and Wilkinson, S. P., "Dielectric Barrier Discharge Plasma Actuators for Flow Control," *Annual Review of Fluid Mech.*, Vol. 66, 2010, pp. 505–529.

[6]Moreau, E., "Airflow control by non-thermal plasma actuators," *Journal of Physics D: Applied Physics*, Vol. 40, 2007, pp. 605–636.

[7]Grundmann, S. and Tropea, C., "Active Cancellation of artificially induced Tollmien-Schlichting waves using plasma actuators," *Exp. in Fluids*, Vol. 44, 2008, pp. 795–806.

[8]Grundmann, S. and Tropea, C., "Experimental damping of boundary-layer oscillations using DBD plasma actuators," *Intl. J. of Heat and Fluid Flow*, Vol. 30, 2009, pp. 394–402.

[9]Gibson, B. A., Arjomandi, M., and Kelso, R. M., "The response of a flat plate boundary layer to an orthogonally arranged dielectric barrier discharge actuator," *J. Phys. D: Appl. Phys.*, Vol. 45, 2012.

[10]Duchmann, A., Kurz, A., Widmann, A., Grundmann, S., and Tropea, C., "Characterization of Tollmien-Schlichting Wave Dampting by DBD Plasma Actuators Using Phase-Locked PIV," *50th AIAA Aerospace Sciences Meeting*, 2012.

[11]Duchmann, A., Reeh, A., Quadros, R., Kriegseis, J., and Tropea, C., "Linear Stability Analysis for Manipulated Boundary-Layer Flows using Plasma Actuators," *Seventh IUTAM Symposium on Laminar-Turbulent Transition*, 2010.

[12]Riherd, M. and Roy, S., "Linear Stability Analysis of a Boundary Layer with Plasma Actuators," *50th AIAA Aerospace Sciences Meeting*, 2012.

[13]Bertolotti, F. P., Herbert, T., and Spalart, P. R., "Linear and nonlinear stability analysis of the Blasius boundary layer," *Journal of Fluid Mechanics*, Vol. 242, 1992, pp. 441–474.

[14]Fasel, H. and Konzelmann, U., "Non-parallel stability of a flat-plate boundary layer using the complete Navier-Stokes equations," *Journal of Fluid Mechanics*, Vol. 221, 1990, pp. 311–347.

[15]Rizzeta, D. P., Visbal, M. R., and Morgan, P. E., "A high-order compact finite-difference scheme for large-eddy simulations of active flow control," *Prog. in Aerospace Sci.*, Vol. 44, 2008, pp. 397–426.

[16]Singh, K. P. and Roy, S., "Force approximation for a plasma actuator operating in atmospheric air," *Journal of Applied Physics*, Vol. 103, 2008.

[17]Boeuf, J. P., Lagmich, Y., Unfer, T., Callegar, T., and Pitchford, L. C., "Electrohydrodynamic force in dielectric barrier discharge plasma actuators," *Journal of Physics D: Applied Physics*, Vol. 40, 2008, pp. 652–662.

[18]Schlichting, H. and Gersten, K., *Boundary Layer Theory, 8^{th} Ed.*, Springer, 2000.

[19]Gaster, M., "A note of the relation between temporally-increasing and spatially-increasing disturbances in hydrodynamics stability," *J. Fluid Mech.*, Vol. 14, 1962, pp. 222–224.

[20]Riherd, M., Roy, S., and Balachandar, S., "Linear Stability Effects of Plasma Actuation on a Zero Pressure Gradient Boundary Layer," *Theoretical and Computational Fluid Dynamics (submitted)*, 2012.

[21]The Mathworks, I., "MATLAB Getting Started Guide, R2011b," 2011.

[22]Wazzan, A. R., Gazley, C., and Smith, A. M. O., "Tollmien-Schlichting waves and Transition: heated and adiabatic wedge flows with applications to bodies of revolution," *Prog. in Aero. Sci.*, Vol. 18, 1979, pp. 351–392.

[23]Gaster, M., "Nonparallel effects on boundary layer stability," *Journal of Fluid Mechanics*, Vol. 66, 1974, pp. 465–480.

[24]Butler, K. M. and Farrell, B. F., "Three-dimensional optimal perturbations in viscous shear flow," *Physics of Fluids A*, Vol. 4, No. 8, 1992, pp. 1637–1650.